

Optical-CDMA in InP

R. G. Broeke, J. Cao, C. Ji, Sang-Woo Seo, Y. Du, N. K. Fontaine, Jong-Hwa Baek, John Yan, F. M. Soares, F. Olsson, S. Lourdudoss, A. V. Pham, M. Shearn, A. Scherer, S. J. B. Yoo

Abstract—This paper describes our InP platforms for photonic integration and the development on these platforms of an ‘Optical Code Division Multiple Access’ system for local area networks. We demonstrate the three building blocks of this system: an optical pulse source, an encoder/decoder pair, and a threshold detector. The optical pulse source consists of an integrated colliding pulse mode laser with nearly transform limited 10Gb/s pulses and optical injection locking to an external clock for synchronization. The encoder/decoder pair is based on arrayed waveguide gratings. Bit error rate measurements involving 6 users at 10Gb/s showed error free transmission, while O-CDMA codes were calibrated using frequency resolved optical gating. For threshold detection after the decoder we compared two MZI based optical thresholding schemes and present results on a new type of electro absorber based MZI.

Index Terms— InP platform, O-CDMA, OAWG, Photonic integrated circuit, MZI, optical thresholding, FROG.

I. INTRODUCTION

PHOTONIC integration has been maturing to a level where system scale functionality can be integrated on a single substrate. Most suitable for advanced photonic integration is the InGaAsP/InP material system, because of its tunable bandgap across the 1.3 μ m and 1.5 μ m communication windows of optical fiber and, therefore, the ability to integrate active and passive waveguides. An InP platform supporting active-passive integration provides three key functionalities on a single substrate: passive optical waveguiding (with bend radii down to 50 μ m to 500 μ m for compact design), phase shifting, and amplification/detection of light. Platforms usually add one or more functionalities like electro-absorption modulators, polarization converters, spot-size converters, on-chip mirrors, or/and electrical high-frequency (HF) phase and HF amplitude modulators. Several InP platforms, using different techniques, have been reported: Quantum well (QW) intermixing [1]

Manuscript received December 14, 2006. This work was supported in part by DARPA and SPAWAR under agreement number N66001-01-1 by JOP-OIDA and HR0011-04-1-0054 supported by DARPA and NSF.

R.G.Broeke, J. Cao, C. Ji, S. W. Seo, Y. Du N. K. Fontaine, J. H. Baek, John Yan, Francisco Soares, A. V. Pham and S. J. B. Yoo are with the Electrical Engineering Department, University of California, Davis, CA 95616 USA, (e-mail: yoo@ece.ucdavis.edu).

F. Olsson and S. Lourdudoss are with the School of Information and Communication Technology, Royal Institute of Technology, KTH-Electrum 229, S-16440, Kista Sweden.

M. Shearn and A. Scherer are with the Division of Engineering and Applied Science, California Institute of Technology, 1200 E. California Boulevard, MC 104-44, Pasadena, CA 91125 USA.

enables active-passive integration without regrowth, but at the expense of increased waveguide loss due to band-tail edge absorption and the introduction of lattice defects by the implanted ions. Butt-joint selective-area (SA) regrowth in combination with a double-etch technique [2-3] provides flexibility in the positioning and type of the active layer and allows for compact design by high contrast waveguide bends. However, it is difficult to control the regrowth of large step butt-joints and to accurately control the etch depth required for the low-contrast waveguides. Integration by symmetric twin-waveguide structure [4] doesn’t require a regrowth, but introduces possible optical absorption in the taper region. Also, the effective index of both waveguides should match accurately to limit taper lengths.

In our approach [5] we use a HVPE lateral regrowth for simultaneous waveguide passivation and planarization. It allows for a noncritical waveguide etching, similar to buried waveguide processes. In this paper we report on two platforms with respect to the development of an integrated O-CDMA system; one platform for low frequency (LF) components and new platform for high frequency (HF). Additional trade-offs in chip design introduced by HF components for rapid code reconfiguration justifies a separate HF platform. Furthermore, we reduced waveguide loss by improved HVPE lateral growth conditions for more uniform sidewall coverage. We employed frequency-resolved optical gating for more accurate optical-phase calibration of the O-CDMA coding/decoding and generating shorter pulses from the mode-locked laser. Finally we introduced a new MZI thresholder design.

We develop the O-CDMA system using a parallel-track approach. On the first track we realize a table-sized optical free space/fiber based system to demonstrate feasibility, principle of operation and to lay the groundwork for system scale characterization. For example, the free-space SLM based 32-user x 10Gb/s O-CDMA system [6]. On the other track we develop the O-CDMA system on an InP platform. The parallel track approach provides an environment, in which we progress towards full integration by inserting InP devices incrementally into an proven operating system architecture. Full integration in semiconductor is a prerequisite for stable and large scale, mobile deployment.

II. INTEGRATION TECHNOLOGY

In this section we give a brief overview of the integrated waveguides in our two platforms, for LF and HF (10 to 40GHz).

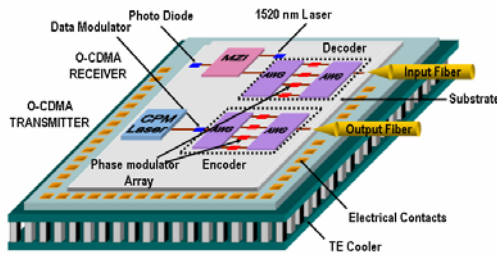


Fig. 1. Schematic picture of fully integrated O-CDMA system.

First, the LF O-CDMA platform; Fig 1 shows a fully integrated O-CDMA system consisting of a transmitter and receiver section. The transmitter consists of a mode-locked laser (MLL) integrated with a spectral-phase encoder. The receiver consists of a decoder integrated with an MZI-based threshold detector (MZI-TD).

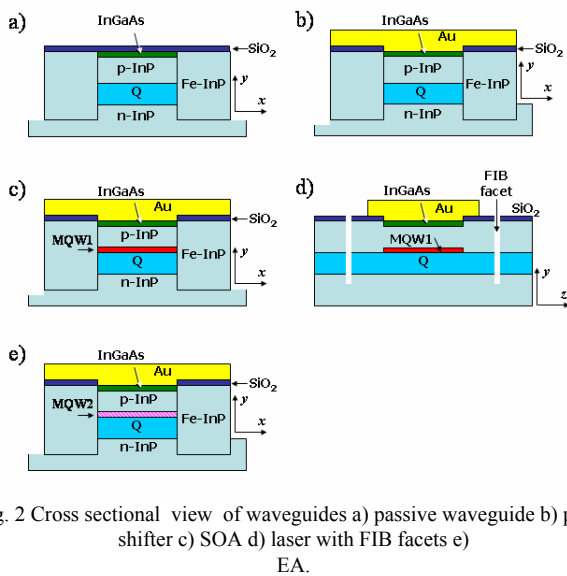


Fig. 2 Cross sectional view of waveguides a) passive waveguide b) phase shifter c) SOA d) laser with FIB facets e) EA.

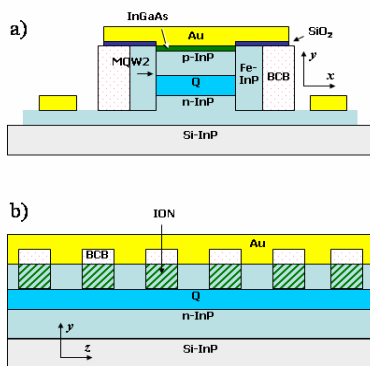


Fig. 3 Traveling-wave phase modulator a) lateral cross section b) longitudinal cross section.

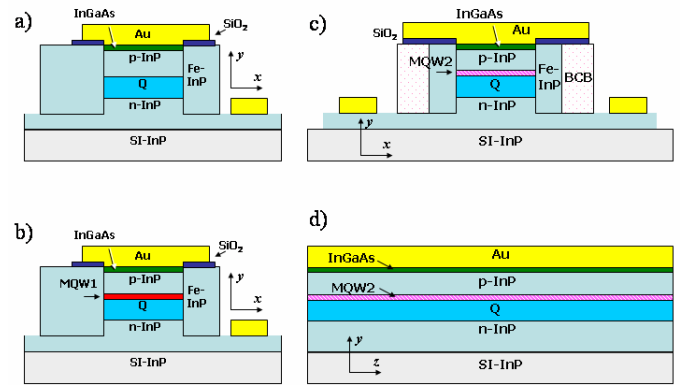


Fig. 4 Cross sections a) phase shifter b) SOA. Cross sections of high frequency EA modulator: c) lateral d) longitudinal.

Fig. 2 shows the cross sectional view of the waveguide types in the O-CDMA devices. The orientation of the cross sections is such that waveguide widths are displayed in the x-direction (lateral), thickness in the y-direction, and the propagation direction of the guided light in the z-direction (longitudinal). Fig. 2a displays a passive waveguide of a 500nm thick quaternary Q(1.15) waveguiding (film) layer sandwiched in InP. Lateral regrown Fe-InP layers passivate the sidewalls of the waveguide and provide electrical isolation. In addition, the lateral regrowth planarizes the waveguide for subsequent metallization steps. Typical waveguide width is 3 μ m, which is a compromise between low propagation loss (2.5dB/cm) and single mode waveguiding (avoiding the symmetrical second order mode). Fig. 2b shows a phase shifter, whose refractive index can be changed by injecting carriers in the guiding layer (forward bias), or by applying an electrical field across the Q layer (reverse bias). The metal (AuGeNi/Au) and highly doped InGaAs layer on top provide a low resistance n-contact for electrical connection to an outside current or voltage source, for instance by wire bonding in packaged devices. Semiconductor optical amplifiers (SOA, Fig. 2c) have multi quantum well (MQW) layer on top of the film layer (MQW1). The MQW1 consists of 6 wells of 7nm thick Q(1.25) InGaAsP and 6nm thick InGaAs barriers. The designed gain peak lies at 1550nm. Fig. 2d shows a longitudinal cross section of a SOA with etched facets. The focused ion beam (FIB) etched facets provide optical feedback for the SOA and create a laser suitable for integration of the laser with other devices on a single substrate. A second type of MQW layer, MQW2 (Fig. 2e) provides a peak gain around 1490nm and has been optimized for electro absorption (EA) modulator operation. For instance for data modulating a pulse train from a 10GHz mode-locked laser, or for phase shifting in a MZI structure, as described later in this paper.

Fast code reconfiguration in the encoder/decoder demands HF traveling-wave phase modulators. These modulator need to be optimized for low propagation loss of HF electrical fields, velocity matching of the optical group and electrical phase velocity, and maximum overlap between the optical fields and the electrical field.

Fig. 3 shows the cross sections of a traveling wave modulator. The most pronounced change with respect to the stack from Fig. 1a is the replacement of the n-doped InP substrate with a semi insulating (SI) substrate. The n-contacts are placed on the top side of the chip, on top of an n-InP buffer layer. This configuration reduces electrical propagation loss by reducing the amount of electrical field in n-doped layers. A benzocyclobutene (BCB) layer on both sides of the Fe-InP provides additional support for the metal contact layer on top. The SiO₂ layers provide an electrically isolated cohesion layer for the metal. Removal of the n-buffer layer between adjacent modulators isolates their n-contacts

The epitaxy on a SI substrate consists of a 500nm thick n-InP buffer layer, a 500nm Q(1.15) layer, a 2.0 μ m p-InP layer with gradually increasing p-doping towards the top, and a 100nm thick InGaAs contact layer. A RIE etch through the Q layer defines the waveguides. A lateral Fe-InP regrowth passivates the waveguides and planarizes the surface. In order to reduce the overlap of the electrical field with the laterally regrown Fe-InP, a wet chemical etch reduces the Fe-InP width to 4 μ m on both sides, which is wide enough not to affect the optical guiding properties of the waveguide. Furthermore, since the microwave electrical field tends to have a lower propagation velocity compared to the optical field, increasing the electrical field confinement in air (by thinner Fe-InP) improves velocity matching. The etching stops at the top of the n-buffer layer to enable the n-contacts.

Fig 3b shows the same modulator, but in a longitudinal cross section through the waveguide center. The segmentation of the p-contact geometry provides velocity matching of the electrical phase with the optical group velocity. The segmentation consists of ion-implantation to locally destroy the conductance of the p-layer and a BCB layer to avoid metal-semiconductor contact on the ion implanted segments.

Due to the SI substrate all electrical contacts need to be placed at the top-side of the device. Fig. 4a shows a LF phase shifter in the HF-platform and Fig.4b a SOA. In case of current injection into the chip, the resistance from the p to n-contact should be minimized. Resistance the n-buffer to the n-contact can be limited to a few Ohms by placing the n-contact as close as possible to the waveguide and by making it sufficiently doped and thick. Fig. 4c and d displays an EA with high speed electrical connections. It is similar to the traveling wave modulator, except that the EA is shorter (up to 300 μ m long), which makes velocity matching much less critical. Hence, no ion implantation is required.

III. O-CDMA ON INP

A SPECTS O-CDMA system employs spectral encoding of ultra-short optical pulses from a mode-locked laser for data transmission. Spectral coding in the transmitter spreads pulses in time at expense of peak power. The decoder only reconstructs the ultra-short, high peak-power pulse if the encoder code and decoder code are conjugates of each other. (The decoder and encoder are similar devices.) The receiver, after the decoder, discriminates correctly decoded pulses from incorrectly decoded pulses by nonlinear threshold detection.

The receiver detects a “1” bit only if a pulse has sufficient peak power (correctly decoded). Otherwise, the receiver detects a “0” bit for a time-spread pulse. The following sections elaborate our results with these InP based O-CDMA components.

A. Mode-locked laser

An ultrafast light source based on semiconductor mode-locked (ML) laser is required for as transmitter in an Optical-CDMA integrated photonic circuit. We have developed a 10 GHz colliding-pulse mode-locked laser (CPM) [8-9] in the platform from Fig.1, allowing for the monolithic integration of the CPM laser with other O-CDMA elements discussed in the rest of the paper. Compared to a regular mode-locked laser design, the CPM laser operates in the configuration where two symmetrically counter-propagating pulses collide and bleach the saturable absorber located at the center of the laser cavity, resulting in deeper saturation and more stable mode locking.

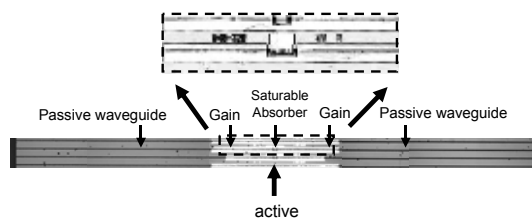


Fig. 5 SEM image of a 10 GHz CPM laser with integrated active-passive waveguides.

Fig. 5 shows the SEM image of a fabricated CPM laser. The required CPM cavity length for 10 GHz operation exceeds 8 mm, which for all all-active design will require fairly high drive current. Furthermore, long (>4 mm) all active mode ML lasers for achieving lower repetition rate tend to suffer from strong pulse shaping effects, resulting in poor chirping and jitter performance [10]. Adopting the active-passive integration process in Fig. 1 allows for reducing the active section length to minimizing these effects and the drive current requirement [8]. The active-passive interfaces are designed to be laterally tilted at 45 deg relative to the waveguide direction. This lateral tilt is critical for eliminating unwanted secondary pulses originating from residual reflections at the interfaces, resulting in much improved mode locking performance compared to the untilted designs. The active region has total length of 2000 μ m, dividing into two gain sections and sandwiching the 45 μ m wide saturable absorber (SA) located at the center. The waveguide is further extended symmetrically on both sides with passive sections, forming the 8200 μ m long laser cavity.

The CPM laser can be synchronized to an external system clock through either electrical hybrid mode locking (HML) [10-11] at the fundamental or a subharmonic frequency, or through the optical synchronous mode locking (OSML) approach [12-13]. In the electrical HML configuration, RF modulation signal is applied to the saturable absorber of the CPM laser through a Ground-Signal-Ground microwave probe,

while the two gain sections and the SA are DC biased through DC needle probes (forward current injection) and the microwave probe (reverse bias voltage) through a bias-tee connection respectively.

CPM laser output pulse characteristics are very sensitive functions of the DC and RF biasing conditions. We utilized the cross-correlation frequency-resolved optical gating (XFROG) technique [14] (Fig. 9) for accurate extraction of the complete temporal amplitude and phase information, and the corresponding spectral domain profiles of the pulse simultaneously.

Fig. 6 shows the XFROG characterization of the CPM laser under two different bias conditions. In Fig. 6a, with 89 mA gain section and -7.5V SA biasing, the tightly distributed XFROG spectrogram indicates that the pulse is close to being transform limited. The extracted time domain intensity and instantaneous frequency profiles in Fig. 6b indicates a pulse width of 5.7 ps with minimal frequency chirp, with time-bandwidth product of 0.67 for a spectral width of 1.8 nm. Fig. 6c shows that the XFROG trace of the same device at a different biasing condition with 156 mA gain section current, -4.5V across the SA. The extracted time domain profile in Fig. 6d shows that the resulting pulse is over 40 ps wide, with both strong linear and higher order chirp components. The XFROG technique allows the full characterization and systematic and efficient optimization of all the individual biasing parameters of a CPM laser in real time.

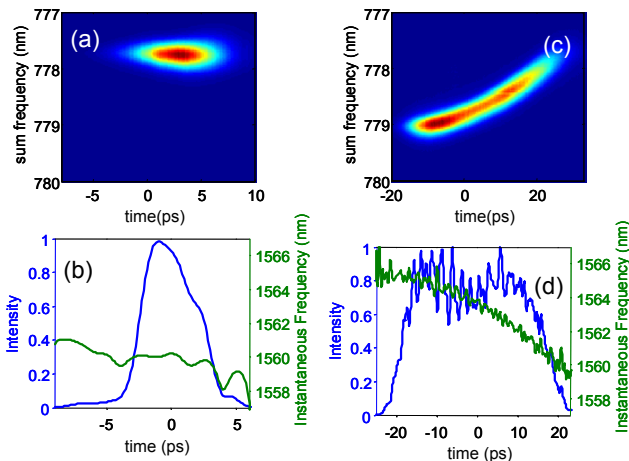


Fig. 6 (a) XFROG spectrogram and (b) extracted time domain intensity and instantaneous frequency of a nearly transform limited pulse; (c) XFROG spectrogram and (d) extracted time domain intensity and instantaneous frequency of a highly chirped pulse from the same CPM laser under different biasing conditions.

We have previously reported in detail the electrical HML investigation of the 10 GHz CPM laser [8]. By applying the RF clock signal matching the passive ML frequency of 10.3 GHz at 19 dBm, we obtained nearly transform limited output with pulse width of 1.75 ps and time-bandwidth product 0.33, with relatively low timing jitter. This short pulse, low chirp performance can be attributed to the careful balancing of the pulse broadening and chirping effects inside the relatively short

gain sections and the SA pulse truncating effects respectively [15]. Minimizing the active-passive interfacial reflections also plays an important role for achieving optimal pulse quality.

For synchronizing remote photonic chip based system nodes in an O-CDMA network, the electrical HML approach, while relatively easy to implement on a single device, requires supplying system clock signal at relatively high RF power to multiple distant locations, and expensive to implement. The alternative OSML approach, would involve the simple routing of a single optical clock signals through the network fiber for injecting locking of all CPM laser sources simultaneously.

For OSML optical injection locking characterization, a commercial tunable mode-locked fiber laser synchronized to an RF synthesizer clock source provides the optical clock, which is coupled into the 10 GHz CPM laser through a polarization-maintaining (PM) attenuator and a lensed fiber. The CPM output, collected through a lensed fiber from the other output facet, passes through a 3 nm tunable filter for removing any residuals of the injection signal, and then routes to different instruments for time and frequency domain measurements, and the Bit-Error-Rate-Tester (BERT) for BER measurements.

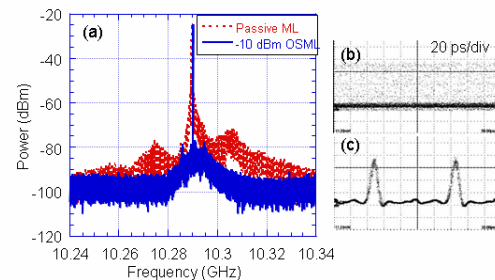


Fig. 7(a) RF power spectra at the fundamental ML frequency of the 10 GHz CPM laser under passive ML and optical injection locking conditions. Also sampling scope traces of the CPM laser output triggered with the RF clock source under (a) passive (b) optical injection locking conditions.

Fig. 7a shows the RF power spectra of a 10 GHz CPM laser under both passive ML and injection locking conditions at -10 dBm coupled optical power, with the injection signal at 1546 nm, 8 nm negatively detuned from the passive ML wavelength. Fig. 7b shows the corresponding 50 GHz optical sampling scope traces, triggered with the RF synthesizer clock. Compared to passive mode-locking the RF spectral lineshape narrows significantly in Fig. 7a under optical injection, corresponding to the sharply reduced timing jitter after synchronization. The estimated RMS timing jitter of the injection-locked CPM laser is 0.5 ps by integrating the single-side-band (SSB) phase noise spectrum, while the injected laser clock signal has RMS jitter of 0.17 ps. The effect of optical injection is primarily phase synchronization, without any observed changes in the pulse width and spectrum of the CPM laser output. Optical phase synchronization effects can be observed at injection power level as low as -23 dBm. BER measurements also demonstrated that the CPM output is error free with $BER < 10^{-11}$ under PRBS $2^{23}-1$ data modulation, demonstrating that optical injection locked 10 GHz CPM laser can indeed serve as a viable short pulse light source in O-CDMA and other photonic integrated circuit applications.

B. InP Encoder and Decoder

Previous integrated O-CDMA encoders are either based on silica arrayed-waveguide gratings (AWG) with non-programmable external phase shifters [16] or based on ring micro-resonators with relatively slow heater based phase shifters [17]. On the other hand, InP platform based SPECTS O-CDMA (Fig. 1) encoders and decoders offer rapid code reconfiguration by employing electro-optical phase shifters and the possibility of realizing monolithically integrated O-CDMA transmitters and receivers [5].

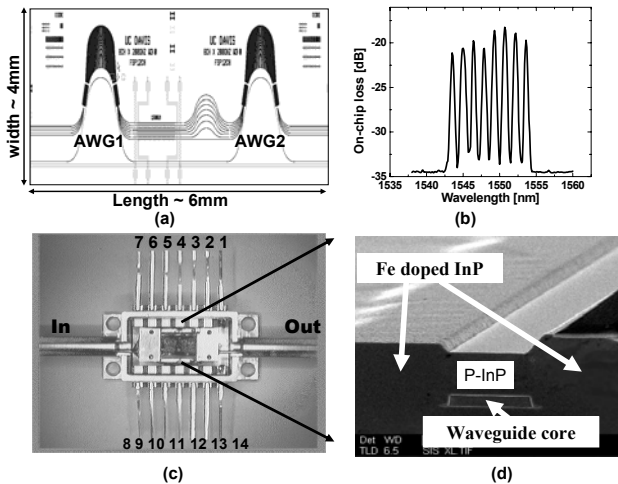


Fig. 8. (a) O-CDMA encoder chip layout, (b) encoder transmission spectrum, (c) packaged O-CDMA encoder chip and (d) SEM picture of laterally regrown passive waveguide.

Fig. 8a shows the O-CDMA encoder mask layout. The AWG pair performs spectral de-multiplexing and multiplexing. Phase modulators (cross section in Fig. 2b) in between the AWGs apply a phase shift, corresponding to the desired O-CDMA code, to each de-multiplexed spectral channel. The input and output waveguides of the device are selected for optimal wavelength match of the two AWGs. Fig. 8b shows the transmission spectrum of an O-CDMA encoder with 32 dB insertion loss. Loss can still be greatly by improving the fiber coupling (here 8dB per fiber-to-chip coupling) and the fabrication process. Fig. 8c and d show the packaged chip and a scanning electron micrograph (SEM) picture of the cross-section of the chip.

One of the challenges is to calibrate the phase response of the individual channels of the InP chip for two reasons. First, the phase-shifter response must be known as a function of injection current or reverse bias voltage (both can be used to generate a phase shift) to apply the right amount of phase shift. Although phase shifter performance can be extracted using test structures, data from the actual shifters in the encoder is preferable due to possible variations between shifters. Second, the chip contains phase errors in the 8 channels due to fabrication tolerances, causing a phase offset. For channel spacings up to ~40GHz (note the encoder chip has 180GHz) the differential phase of the channels can be extracted by detecting the coherent beating

between two spectral channels of the encoder [18]. This approach requires the precise alignment of two axial modes from a mode-locked laser signal with two encoder channels. The two modes produce a coherent beating response at the encoder output. However, this beating is hard to detect beyond 40GHz without sophisticated high-speed electronics. In contrast, we characterized the phase response of the 180 GHz encoder chip using the X-FROG technique [19], which avoids the precision spectral alignment requirements in the coherent beating approach. Also, the phase information off all channels is acquired in a single measurement.

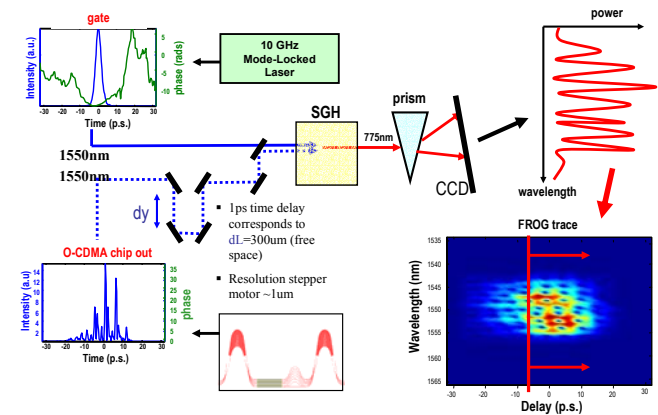


Fig. 9. Setup for X-FROG based phase error measurement.

Fig. 9 shows the principle of X-FROG based phase error measurement. The ML laser and compressor generated 0.5 ps pulses with a repetition rate of 10 GHz. A polarization controller (PC) put the pulses in TE polarization before a lensed fiber injected them into the encoder chip at 10dBm. At the chip output, an EDFA amplified the output pulse and fed it into the X-FROG through a PC. The amplified uncompressed pulse of the mode-locked laser served as reference for the X-FROG.

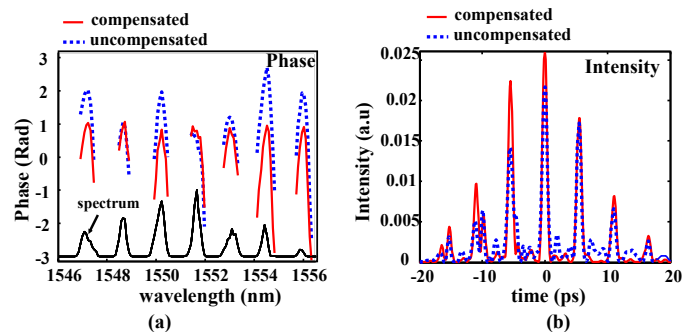


Fig. 10. (a) Phase and (b) Intensity response of phase-compensated encoder.

Fig. 10a shows the retrieved phase information (curve at the bottom corresponds to power in the channels), and 10b the encoder output. The dotted lines in Figs. a and b are without phase error compensation, solid/red lines with (by reverse-biasing the phase shifters). After compensation, the phases of all channels (peak of solid/red lines) are almost flat (Fig.10a). The compensation clearly improves the peak power and signal to noise ratio (Fig 10b). The ringing peaks at 5.5 ps spacing originate from the 180GHz comb-shaped spectral response of the AWG (Fig. 8b). This phase compensation result shows both the proper operation of the InP encoder and the value of FROG as encoder characterization tool.

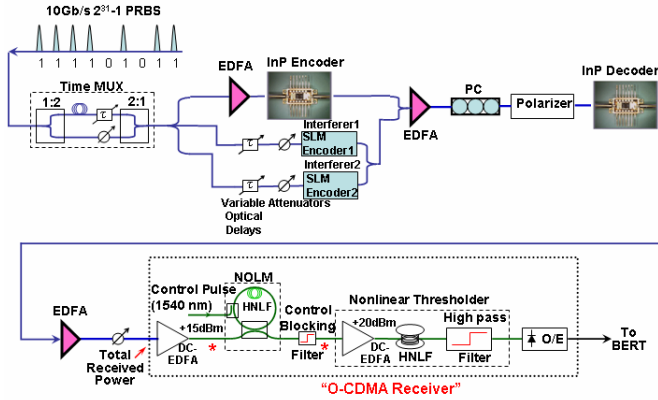


Fig. 11. Experimental setup for 6 x 10Gb/s O-CDMA testbed.

Fig. 11 shows the schematic of the O-CDMA testbed. The mode-locked fiber laser source generated a 500-fs-pulse train at a 10 GHz repetition rate. A LiNbO₃ modulator modulated the pulse train with a 10 Gb/s 2³¹-1 pseudo-random bit sequence (PRBS) pattern. A time-mux splitted the modulated train into two time slots of 50 ps each. A dispersion-compensated erbium-doped fiber amplifier (DC-EDFA) boosted the train, which is subsequently spatially split into three branches. One branch passes through the InP encoder [20] as the intended user (user channel). The other two branches are encoded by spatial light modulator (SLM) encoders [6], which acted as independent interferers (IF1 and IF2). The SLM encoders contained variable time delays for synchronization. After encoding, the intended user and interferers were combined and routed to the InP decoder. Upstream to each chip, an erbium doped fiber amplifier (EDFA) followed by a polarization controller supplied 21 dBm of transverse electric (TE) polarized light.

The InP devices each consist of an identical pair of 8-channel AWGs with 180 GHz channel spacing and a free spectral range (FSR) of 12-channel spacings. The 1.4 THz wavelength span provided by the 8 channels is sufficient for encoding sub-picosecond (~0.5 ps) pulses. The InP devices are packaged in a standard 14-pin butterfly package with temperature control, which allows for an exact wavelength match of the encoder and decoder. The 2000um long phase-shifters are controlled by electrically biasing wire-bonded electrical leads.

We selected the 8-chip Walsh code [21] set for our spectral phase coding experiment. The InP encoder applies code W1 containing the bits [11111111], whereas the InP decoder applies conjugate code (*) W1* [00000000]. Here 1 denotes π Radians phase shift and 0 denotes 0 phase shift in the respective phase shifters. SLM interferers IF1 and IF2 apply W2 [10101010] and W4 [10011001], respectively. These codes were selected for optimal suppression of the multi user interference (MUI). The gate (a nonlinear optical loop mirror (NOLM), to be replaced by the integrated MZI) is followed by power thresholding with highly nonlinear fiber (HNLf) and a long-pass filter. This combination suppresses an incorrectly

decoded signal while it passes a correctly decoded signal.

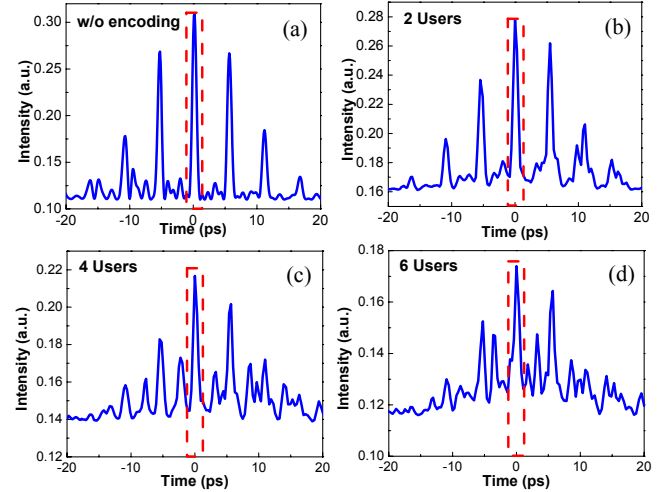


Fig. 12. The time domain cross-correlation traces of the correctly decoded signal for (a) without coding, (b) 2 users, (c) 4 users and (c) 6 users.

Fig. 12 displays the effect of MUI on the pulse output. Fig.12a shows the cross-correlation trace after the encoder-decoder pair with phase error compensation but without coding. The ~3ps time-gating around t = 0ps (dotted line) removes the ringing peaks at the expense of signal power. Fig. 12b shows the cross-correlation trace of the output of the encoder-decoder pair without interferers (extra users), with W1 and W1* codes for encoder and decoder for 2 time slots. Fig. 12c and 12d show the traces with added interferer W2 and interferers W2 and W4, respectively (two time slots).

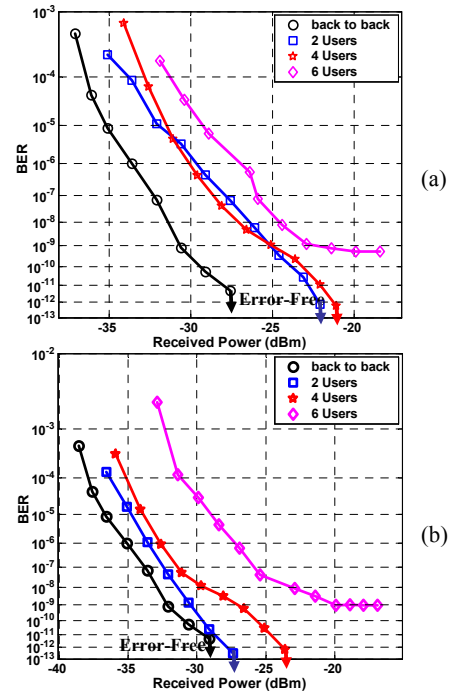


Fig. 13. BER measurement results for (a) InP encoder and decoder chips and (b) SLM encoders and decoder.

Fig. 13a shows the BER measurement results for the 6-user

O-CDMA system with InP encoder and decoder. Back-to-back data were taken with the O-CDMA encoder and decoder pair bypassed. Received power in all BER curves is defined as the average input power per user as measured at the input of the “O-CDMA receiver”. The 2-user and 4-user experiments demonstrated error-free operation and a power penalty of 5.5 dB at BER = 10⁻⁹ with respect to back-to-back. The penalty can be mainly attributed to power lost to the ringing peaks. The 6-user case attained an error floor at 10⁻⁹, primarily due to MUI inside the time gate. MUI effects are relatively small for 2 and 4 users, resulting in no observable noise floor. For a narrower time gate window and/or longer code length would mitigate the MUI effects significantly and an error-free operation is expected.

In order to investigate the effect of the spectral filtering and loss in the InP based en/decoders, we repeated the BER measurement but replaced the InP devices with SLM based en/decoders. SLM devices approach ideal coding performance due to their rectangular filter shape. Fig. 13b shows the BER measurement result and eye diagrams. The 2-user and 4-user experiments demonstrated error-free operation with a power penalty of 2 dB and 5 dB, respectively, at BER = 10⁻⁹. The error floor below 10⁻⁹ in the 6-user SLM case confirms that MUI and not the InP chip response is the dominant limitation for error-free operation of O-CDMA system.

C. MZI threshold detector development

The last step of the SPECT-O-CDMA transmission link requires non-linear optical thresholding: the detection of properly decoded optical pulses with narrow pulse width and high peak power, and the blocking of the time spread improperly decoded interferer signal. Compared to other nonlinear fiber based thresholder approaches, The MZI thresholder is less bulky, more sensitive [22-23] and is compatible with monolithic integration with other semiconductor components. Here we describe an improved “clock-gated” MZI scheme with respect to the “self-gated” approach reported previously [5]. Both schemes depend on differential operation of the MZI.

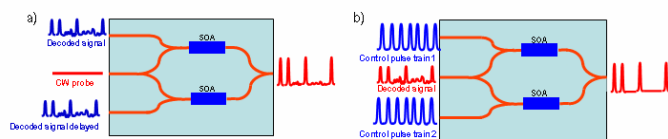


Fig. 14 O-CDMA thresholder in a) non-gated b) clock-gated configuration

Fig. 14 shows the self-gated and clock-gated MZI operation. In the self-gated scheme, no external clock signal is provided. The decoded pulse is split in two and each part enters a distinct MZI arm with a time delay. Only the correctly decoded pulses have sufficiently fast rising edges to saturate the non-linear optical elements in the MZI arms, opening a differential gate for the CW probe signal. The clock-gated scheme uses the external short pulse clock signal for generating the differential

gate of the MZI.

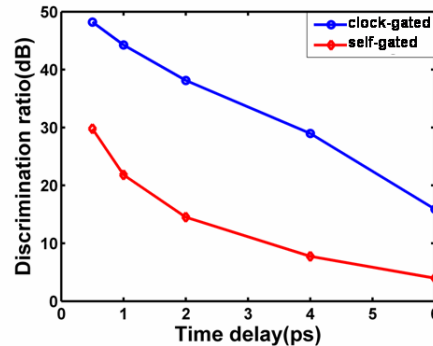


Fig. 15. Graph of power ratio after MZI thresholder for self-gated and clock-gated operations.

Fig. 15 shows the simulated discrimination ratio (the ratio of the integrated energy of a correctly decoded pulse vs. that of an incorrectly decoded pulse) as a function of the time delay between the two MZI arms for non-gated and clock-gated operation using 64-bit Walsh codes. Clock-gating outperforms self-gating by up to 20 dB, because the in the self-gated condition a partial broad gate can still be present for incorrectly decoded signal, resulting in incomplete blocking.

For improved performance, we investigated a new class of integrated MZI, based on reverse biased electro-absorbers (EA) [24]. The reverse biased EA sections result in faster carrier sweep out (tens of ps) and less Amplified Stimulated Emission (ASE) noise compared to the conventional forward biased SOAs in the MZI arms, favoring high speed, lower power consumption operation with greater cascadability.

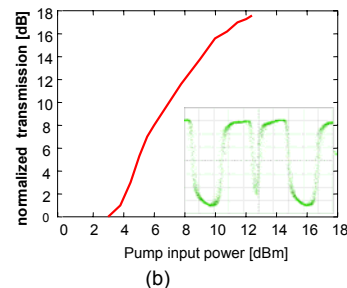
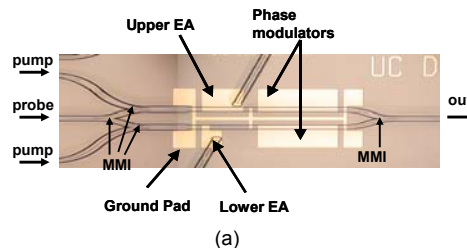


Fig. 16 a) Photograph of fabricated EA-MZI with active-passive integrated waveguide. b) Normalized MZI transmission vs. pump input power, (inset) showing EA-MZI output at 2.5Gb/s.

Fig. 16a shows the fabricated EA-MZI with four multi-mode interference (MMI) based 3 dB couplers, two active EA sections of 200 um and 50 um in length and two 600 um long phase shifters (see also Fig 2). The phase modulators allow the MZI to be biased for optimal destructive interference at the

MZI output, whereas the unequal EA section lengths allow better power balance between the two arms (without pump). Injection of an optical pump signal into the shortest EA induces cross phase and amplitude modulation, and the device operates as a ‘non-inverting’ optical switch (or wavelength converter).

Fig. 16b shows the normalized MZI switching output vs. pump input power with the pump signal at 1540 nm, probe signal at 1550 nm, and the upper and lower EA reverse biased at -1 V and -12 V respectively. A 10 dB pump power change (ER) resulted in 18 dB output switching ratio, demonstrating the optical signal regeneration capability of the EA-MZI. Fig. 16b inset shows the MZI wavelength conversion output from a 2.5 Gb/s 2^7-1 pseudo-random-bit-sequence pump input. These results demonstrate the optical switching capacity of the EA-MZI device, and its potential as a high speed, low power, and low noise optical threshold element.

IV. FUTURE WORK

A monolithically integrated on-chip system is a challenging task to achieve. To make the on-chip O-CDMA system operate properly, several key issues need to be addressed. These include low-loss waveguide, the realization of narrow channel spacing AWG, on-chip mirror for lasing operation of mode-locked laser. By optimizing the layer stack of the material system of the device and processing procedure of the fabrication, we achieved 3dB/cm for passive waveguide for doped material. This low loss waveguide combined with on-chip amplification by using SOA can satisfy the requirement for integrated system. We will discuss two other issues in this section:

A. Realization of narrow channel count AWG

For O-CDMA the amount of users can be increased if the (AWG) channel spacing is reduced or if the band width of the laser pulses is increased. The narrower the channel spacing, longer code length can be applied to allow better suppression of MUI [5]. Currently we are working toward 50GHz and 20GHz channel spacing encoders. As intermediate step we have developed a 100 GHz channel spacing AWG to optimize the layer stack, fabrication processing step and AWG design parameters (such as input/output free-propagation region and waveguide shape).

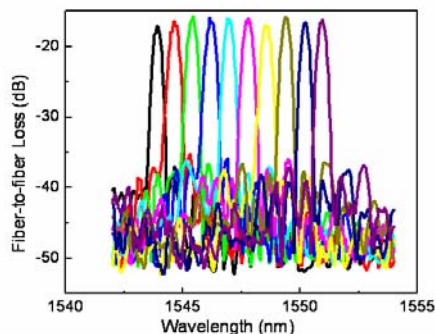


Fig. 17. a) transmission spectra of all 10 transmission channels of 100GHz channel spacing AWG

Fig. 17 shows the transmission spectrum of a 10 channel x 100GHz channel spacing AWG. The FSR of this AWG is 12.8nm which is the same as our 8-channel device. The 3dB bandwidth of single channel is 0.35nm. The fiber to fiber loss of this single AWG is 16dB. The signal to noise ratio (SNR) is more than 25dB and side-lobe suppression is about 20dB. The channel spacing is 0.8nm. The central wavelength (channel 6) is 1547.7nm. The non-uniformity among 10 channels is less than 2dB. Compared to 8-channel x 200GHz channel spacing device, the fiber-to-fiber loss of the 100GHz design does not increase. This proves that the improved design allows narrower channel spacings without performance loss, making higher channel count AWGs feasible. Furthermore, we have characterized the phase errors in the AWG arms using a new method: XFROG in combination with an inverse Fourier transform. Knowledge of these errors will enable us to reduce systematic phase errors in the AWG arms.

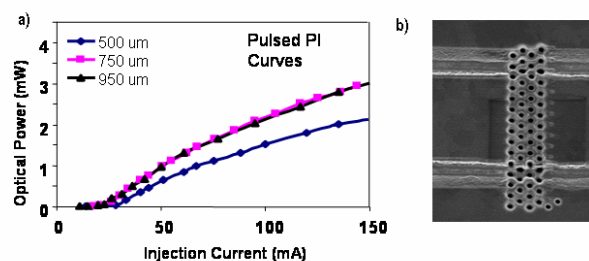


Fig. 18 a) Optical output of etched facet laser vs. injection current (1% duty cycle), and b) Focus-Ion-Beam etched photonic crystal laser mirror.

B. On-chip mirror for mode-locked laser integration

Monolithic integration of the CPM laser source with other elements requires the development of build-in mirror reflectors (Fig. 2d). We are developing the photonic crystal (PC) based laser mirrors similar to that demonstrated on CW semiconductor lasers [25]. Etched mirrors allow for accurate control of the repetition rate. Fig. 18b shows the photonic crystal mirrors fabricated using focused-ion-beam (FIB) and titanium etch mask. Fig. 18a displays pulsed laser output for three laser cavities having different lengths. Lasing threshold currents observed were around 25 mA (1% duty cycle). Analyses of the Fourier components of the output spectra confirmed lasing action in the cavity defined by the etched mirrors instead in between the anti reflection coated cleaved facets.

V. CONCLUSION

InP platforms have huge potential to provide compact and stable monolithic integration for system scale applications. We presented two InP integration platforms and demonstrated up to 60Gb/s O-CDMA using InP encoders/decoders. Adding our results on the 10Gb/s mode-locked laser transmitter with nearly transform limited 1.75 ps pulses and the EA-based MZI threshold detector we firmly believe in the feasibility of a single O-CDMA transceiver chip with transmission capacity beyond 100Gb/s. Future work involves improved channel count, by denser spectral resolution of the O-CDMA system and shorter mode-locked laser pulses for wider pulse spectra.

ACKNOWLEDGMENT

REFERENCES

- [1] E. J. Skogen, J. W. Raring, G. B. Morrison, C. S. Wang, V. Lal, M. L. Masanovic, and L. A. Coldren, "Monolithically integrated active components: a quantum-well intermixing approach," *Selected Topics in Quantum Electronics, IEEE Journal of*, vol.11, no.2pp. 343- 355, March-April 2005
- [2] J.J.M. Binsma, J.H. den Besten and R.G. Broeke, "InP-based Photonic Integration Technology," in *Optical Amplifiers and Their Applications / Integrated Photonics Research Topical Meetings on CD-ROM* (The Optical Society of America, Washington, DC, 2004), IFB1.
- [3] E. Bente and M. Smit, "Ultra Fast InP Integrated Circuits," *Proceedings of SPIE*, Vol. 6124, 612419-44, 2006
- [4] Forrest, S.R.; Gokhale, M.R.; Studenkov, P.V.; Fengnian Xia, "Integrated photonics using asymmetric twin-waveguide structures," *Indium Phosphide and Related Materials, 2000. Conference Proceedings. 2000 International Conference on*, vol., no.pp.13-16, 2000
- [5] C. Ji, R. G. Broeke, Y. Du, J. Cao, N. Chubun, P. Bjeletich, F. Olsson, S. Lourdudoss, R. Welty, C. Reinhardt, P. L. Stephan, and S. J. B. Yoo, "Monolithically integrated InP based photonic chip development for O-CDMA systems," *IEEE J. Select. Topics Quantum Electron.*, vol. 11 (1), pp. 66-77, 2005.
- [6] V. J. Hernandez, W. Cong, J. Hu, C. Yang, N. K. Fontaine, R. P. Scott, Z. Ding, B. H. Kolner, J. P. Heritage, and S. J. B. Yoo, "A 320-Gb/s Capacity (32-User X 10 Gb/s) SPECTS O-CDMA Network Testbed with Enhanced Spectral Efficiency Through Forward Error Correction," accepted for *IEEE/OSA Journal of Lightwave Technology*, Nov. 2006.
- [7] R. P. Scott, N. K. Fontaine, J. P. Heritage, B. H. Kolner, and S. J. B. Yoo, "3.5-THz Wide, 175 Mode Optical Comb Source," in *Technical Digest of IEEE/OSA Optical Fiber Communication Conference*, paper no. OWJ3, 2007.
- [8] C. Ji, N. Chubun, R. G. Broeke, J. Cao, Y. Du, S. J. B. Yoo, K. Y. Liou, J. R. Lothian, S. Vatanapradit, S. N. G. Chu, B. Patel, W. S. Hobson, and W. T. Tsang, "Synchronized transform-limited operation of 10-GHz colliding pulse mode-locked laser," *IEEE Photonics Technology Letters*, vol. 18, pp. 625-7, 2006.
- [9] Y. K. Chen and M. C. Wu, "Monolithic colliding-pulse mode-locked quantum-well lasers," *IEEE Journal of Quantum Electronics*, vol. 28, pp. 2176-85, 1992.
- [10] K. Yvind, D. Larsson, L. J. Christiansen, J. Mork, J. M. Hvam, and J. Hanberg, "High-performance 10 GHz all-active monolithic modelocked semiconductor lasers," *Electronics Letters*, vol. 40, pp. 735-7, 2004.
- [11] H. Fan, C. Wu, M. El-Aasser, N. K. Dutta, U. Koren, and A. B. Piccirilli, "Colliding pulse mode-locked laser," *IEEE Photonics Technology Letters*, vol. 12, pp. 972-3, 2000.
- [12] S. Arahira and Y. Ogawa, "480-GHz subharmonic synchronous mode locking in a short-cavity colliding-pulse mode-locked laser diode," *IEEE Photonics Technology Letters*, vol. 14, pp. 537-9, 2002.
- [13] H. Kurita, T. Shimizu, and H. Yokoyama, "Experimental investigations of harmonic synchronization conditions and mechanisms of mode locked laser diodes by optical pulse injection," *IEEE Journal of Selected Topics in Quantum Electronics*, vol. 2, pp508-513, 1996.
- [14] R. Trebino, "Frequency resolved optical gating: the measurement of ultrashort laser pulses," Kluwer Academic Publishers, Boston, 2000.
- [15] S. Gee, R. Coffie, P. J. Delfyett, G. Alphonse, J. Connolly, "Intracavity gain and absorption dynamics of hybrid modelocked semiconductor lasers using multiple quantum well saturable absorbers," *Appl. Phys. Lett.* 71, pp 2569-2571, 1997.
- [16] H. Tsuda, H. Takenouchi, T. Ishii, K. Okamoto, T. Goh, K. Sato, A. Hirano, T. Kurokawa, and C. Amano, "Spectral encoding and decoding of 10 Gbit/s femtosecond pulses using high resolution arrayed-waveguide grating," *IEE Electron. Lett.*, vol. 35(14), pp. 1186-8, 1999.
- [17] A. Agarwal, P. Toliver, R. Menendez, S. Etemad, J. Jackel, J. Young, T. Banwell, B. E. Little, S. T. Chu, W. Chen, W. Chen, J. Hryniewicz, F. Johnson, D. Gill, O. King, R. Davidson, K. Donovan, and P. J. Delfyett, "Fully programmable ring-resonator-based integrated photonic circuit for phase coherent applications," *IEEE J. Lightwave Technol.*, vol. 24(1), pp. 77-87, 2006.
- [18] A. Agarwal, P. Toliver, R. Menendez, S. Etemad, J. Jackel, J. Young, T. Banwell, B. E. Little, S. T. Chu, P. Delfyett, "Fully-programmable ring resonator based integrated photonic circuit for phase coherent applications," *OFC 2005, PDP6*, 2005.
- [19] R. G. Broeke, J. Cao, N. K. Fontaine, C. Ji, N. Chubun, F. Olsson, S. Lourdudoss, B. H. Kolner, J. P. Heritage, and S. J. B. Yoo, "Phase Characterization of an InP based Optical-CDMA Encoder Using Frequency-Resolved Optical Gating (FROG)," in *Technical Digest IEEE LEOS Annual Meeting*, pp. ML2, 2005.
- [20] J. Cao, R. G. Broeke, N. Fontaine, C. Ji, Y. Du, N. Chubun, K. Aihara, Anh-Vu Pham, F. Olsson, S. Lourdudoss, and S. J. B. Yoo, "Demonstration of spectral phase O-CDMA encoding and decoding in monolithically integrated Arrayed-Waveguide-Grating-Based Encoder," to be published in *IEEE Photon. Technol. Lett.*, 2007.
- [21] F. J. MacWilliams and N. J. A. Sloane, "The Theory of Error Correcting Codes," New York: North-Holland, 1977.
- [22] H. P. Sardesai and A. M. Weiner, "Nonlinear fibre-optic receiver for ultrashort pulse code division multiple access communications," *Electron. Lett.*, vol. 33, pp. 610-11, 1997.
- [23] Z. Jiang, et al., "Spectrally coded O-CDMA system with four users at 2.5 Gbit/s using low power nonlinear processing," *Electron. Lett.*, vol. 40, pp. 623-5, 2004.
- [24] M. Suzuki, H. Tanaka, S. Akiba, "Effect of hole pileup at heterointerface of modulation voltage in GaInAsP electroabsorption modulators," *Electron. Lett.* 25. pp88-89. 1989.
- [25] J. Moosburger, M. Kamp, F. Klopff, J. P. Reithmaier, A. Forchel, "semiconductor lasers with 2D Photonic Crystal Mirrors based on a wet-oxidized Al₂O₃-mask", *IEEE Photonics Technology Letters*, vol. 13, pp. 406-408, 2001.

Ronald Broeke received the M.S. degree in physics from the University of Utrecht, The Netherlands in 1998. He received his Ph.D. degree from the Department of Electrical Engineering, Delft University of Technology, Delft, The Netherlands in 2003. He is currently a Postdoctoral Research Scientist with the Department of Electrical and Computer Engineering, University of California Davis.

Jing Cao (S'01) received his B.S. and M.S degrees from the Department of Electronics Engineering, Tsinghua University, China in 1997, 2000 respectively. He is now a graduate student in ECE Department of UC, Davis. His research focuses on optical integrated devices and system integration for next generation optical network.

Mr. Cao is a member of OSA.

Chen Ji received the B.S. degree in physics from the University of Illinois, Urbana-Campaign, in 1993, and the Ph.D. degree in Physics in electrical engineering from Cornell University, Ithaca, NY, in 1999

He is currently a Postdoctoral Research Scientist with the Department of Electrical and Computer Engineering, University of California Davis. His research interests include semiconductor lasers, optical integrates devices, and system integration for next generation optical networks.



Sang-Woo Seo (M '03) received the B.S. degree in electrical and computer engineering from Ajou University, Korea, in 1997, the M.S. in information and communications from Kwangju Institute of Science and Technology (KJIST), Korea, in 1999, and the Ph.D. in electrical and computer engineering from Georgia Institute of Technology, Atlanta, Georgia, in 2003.

From 2003 to 2005, He worked at Georgia Tech and Duke University as a research engineer on the heterogeneous integration and characterization of thin film photonic devices for multispectral imaging, fully embedded high-speed optical interconnections and sensors. Since 2005, He has been working on high-speed modulators, photonic integrated devices, and system integration for optical code division access network and optical arbitrary waveform generation at University of California, Davis.

Yixue Du (S'03) received the M.S. degree in physics from Oklahoma State University, Stillwater, OK., in 1998. She is currently working toward the Ph.D. degree in electrical engineering at the University of California, Davis. Her research interests include simulation of the network behavior and the design

and testing of non-linear optical thresholding device in optical-code-division multiple-access networks.

Nick K. Fontaine received the B.S. degree in Electrical Engineering and a B.S. degree in Optical Engineering from the University of California, Davis in 2004. He is currently a Ph.D. student at the University of California, Davis. His research interests are frequency resolved optical gating (FROG), optical arbitrary waveform generation, optical code-division multiple access, and very small lasers.



Jong-Hwa Baek received the M.S. and Ph.D. degrees in the Department of Physics from Korea Advanced Institute of Science and Technology, Daejeon, Korea, in 1999 and 2004, respectively.

He is currently a Research Scientist at the University of California at Davis. His research interests include photonic integrated circuits, photonic crystal active devices, and nano-photonics technologies.



John Yan received the B.S. degree in electrical engineering from the University of California, Davis in 2005 and is currently pursuing his Ph.D. at the same school. His research interests include optical semiconductor integration, radio frequency ICs and mixed signal ICs.

John Yan is a member of Tau Beta Pi.

Francisco M. Soares received the M.S. in Electrical Engineering from the Delft University of Technology, the Netherlands, in 2000. In 2006, he received the Ph.D. degree from the Department of Electrical Engineering, Technical University of Eindhoven, The Netherlands, on InP-based integrated optical beamformers for phased-array antennas and InP-based spot-size converters for improved fiber-chip coupling.

In 2006, he joined the University of California at Davis where he is engaged in research on optical arbitrary waveform generators in InP technology. His major fields of interest are theories, modeling, characterization, and fabrication of compound semiconductor devices, such as optical switches and modulators, arrayed waveguide gratings, spot-size converters, and multi-mode interference couplers.



Anh-Vu H. Pham (SM'03) received the B.E.E. (with highest honors), M.S., and Ph.D. degrees from the Georgia Institute of Technology, Atlanta, in 1995, 1997, and 1999, respectively.

In 1997, he co-founded RF Solutions, LLC, an RFIC company that was acquired by Anadigics in 2003. He has held faculty positions with Clemson University and the

University of California at Davis, where he is currently an Associate Professor. He has coauthored ~80 technical papers. His research interests are in the area of RF and high-speed packaging and signal integrity, and RFIC design.

Prof. Anh-Vu serves as a member of the IEEE Microwave Theory and Techniques Society (IEEE MTT-S) International Microwave Symposium (IMS) Technical Program Committee (TPC) on Power Amplifiers and Integrated Circuits. He has been the chair of the IEEE MTT-12 Microwave and Millimeter Wave Packaging and Manufacturing Technical Committee of the IEEE MTT-S. He was the recipient of the 2001 National Science Foundation CAREER Award. He is also active as a consultant to the industry.

Fredrik Olsson received the B.S. degree in physics from KTH, Royal Institute of Technology, Stockholm, Sweden, in 2000. He is currently working towards the Ph.D. degree at the School of Information and Communication Technology, at KTH. His research interests include integration of III/V semiconductor materials on silicon and growth of optical integrated devices.

S. Lourduodoss (M'97-SM'99) received the M.S. degree in chemistry from Madras University, Madras, India, in 1976 and the Ph.D. degree in chemistry from Faculté Libre des Sciences de Lille, Lille, France, in 1979.

As a Postdoctoral Fellow at KTH, Stockholm, Sweden, he worked on the thermochemical aspects of thermal energy storage and absorption heat pumps until 1985. Afterwards, he started to work on the epitaxial growth and characterization of III-V semiconductors for device fabrication at Swedish Institute of Microelectronics, Kista, Sweden. Along with his colleagues, he developed an attractive semi-insulating regrowth technology by HVPE for

integration and high speed device fabrication. Currently, he is a Professor of semiconductor materials at KTH and is involved in undergraduate and graduate education. His research interests include MOVPE of GaN and related materials and the issues related to the monolithic integration of III-V materials on single platform as well as on Si by HVPE.



Michael Shearn received B.S. degrees in electrical engineering, physics, and mathematics from Southern Methodist University in Dallas, Texas, in 2004. He is currently a Ph.D. student in Applied Physics at the California Institute of Technology in Pasadena, California. His research interests include silicon photonics, optical resonators, and novel fabrication techniques.



Axel Scherer received the B.S., M.S., and Ph.D. degrees from the New Mexico Institute of Mining and Technology, Socorro, New Mexico, in 1981, 1982, and 1985, respectively. From 1985 until 1993, he worked in the Quantum Device Fabrication Group at Bellcore. Currently, he is the Bernard E. Neches Professor of Electrical Engineering, Applied Physics, and Physics at the California Institute of Technology,

Pasadena, specializing in device microfabrication. His research interests include design and fabrication of functional photonic, nanomagnetic, and microfluidic devices.

S. J. Ben Yoo (S'82-M'84-SM'97) received the B.S. degree in electrical engineering with distinction, the M.S. degree in electrical engineering, and the Ph.D. degree in electrical engineering with minor in physics, all from Stanford University, Stanford, CA, in 1984, 1986, and 1991, respectively.

He currently serves as Professor of Electrical Engineering at University of California at Davis (UC Davis) and Director of UC Davis branch CITRIS (Center for Information Technology Research in the Interest of Society). His research at UC Davis includes high-performance all-optical devices, systems, and networking technologies for the next generation Internet. In particular, he is conducting research on architectures, systems integration, and network experiments related to all-optical label switching routers and optical code division multiple access technologies. Prior to joining UC Davis in 1999, he was a Senior Research Scientist at Bell Communications Research (Bellcore), leading technical efforts in optical networking research and systems integration. His research activities at Bellcore included optical-label switching for the next-generation Internet, power transients in reconfigurable optical networks, wavelength interchanging cross connects, wavelength converters, vertical-cavity lasers, and high-speed modulators. He also participated in the advanced technology demonstration network/multiwavelength optical networking (ATD/MONET) systems integration, the OC-192 synchronous optical network (SONET) ring studies, and a number of standardization activities which led to documentations of *Generic Requirements*, GR-2918-CORE (1999), GR-2918-ILR (1999), GR-1377-CORE (1995), and GR-1377-ILR (1995) on dense WDM and OC-192 systems. Prior to joining Bellcore in 1991, he conducted research at Stanford University on nonlinear optical processes in quantum wells, a four-wave-mixing study of relaxation mechanisms in dye molecules, and ultrafast diffusion-driven photodetectors. During this period, he also conducted research on lifetime measurements of intersubband transitions and on nonlinear optical storage mechanisms at Bell Laboratories and IBM Research Laboratories, respectively.

Prof. Yoo is a Fellow of IEEE Lasers & Electro-Optics Society (LEOS), a Fellow of the Optical Society of America (OSA), and a Member of Tau Beta Pi. He is a recipient of the DARPA Award for Sustained Excellence in 1997, the Bellcore CEO Award in 1998, and the Mid-Career Research Faculty Award (UC Davis) in 2004. Prof. Yoo has served as Co-Chair of Technical Program Committee for APOC 2004 and APOC 2003, and Technical Program Committee Member for CLEO'2005, CLEO'2004, CLEO'2003, LEOS'2000, LEOS'1999, LEOS'1998, OECC/COIN'2004, COIN'2003, COIN'2002, NLGA'2000, and OAA'2005. He is General Co-Chair for IEEE LEOS Photonics in Switching conference 2007. Prof. Yoo also serves as Associate Editor for IEEE Photonics Technology Letters, and Guest Editor for IEEE/OSA Journal of Lightwave Technology (2005) and IEEE Journal of Special Topics in Quantum Electronics (2007).